doi:10.1016/j.jmb.2005.12.034 J. Mol. Biol. (2006) 356, 982–992

JMB

Available online at www.sciencedirect.com

SCIENCE DIRECT®

ELSEVIER

Folding Transitions During Assembly of the Eukaryotic mRNA Cap-binding Complex

Tobias von der Haar[1,2]*, Yuko Oku[3], Marina Ptushkina[1], Nathan Moerke[4] Gerhard Wagner[4], John D. Gross[3] and John E. G. McCarthy[1]

[1]*Manchester Interdisciplinary Biocentre, c/o Jackson's Mill University of Manchester P.O. Box 88, Manchester M60 1QD, UK*

[2]*Department of Biosciences University of Kent, Canterbury CT2 7NJ, UK*

[3]*Department of Biochemistry and Molecular Pharmacology University of Massachusetts Medical School, LRB 922 364 Plantation Street, Worcester MA 01604, USA*

[4]*Department of Biological Chemistry and Molecular Pharmacology, Harvard Medical School, Boston, MA 12115, USA*

**Corresponding author*

The cap-binding protein eIF4E is the first in a chain of translation initiation factors that recruit 40 S ribosomal subunits to the 5′ end of eukaryotic mRNA. During cap-dependent translation, this protein binds to the 5′-terminal m^7Gppp cap of the mRNA, as well as to the adaptor protein eIF4G. The latter then interacts with small ribosomal subunit-bound proteins, thereby promoting the mRNA recruitment process. Here, we show apo-eIF4E to be a protein that contains extensive unstructured regions, which are induced to fold upon recognition of the cap structure. Binding of eIF4G to apo-eIF4E likewise induces folding of the protein into a state that is similar to, but not identical with, that of cap-bound eIF4E. At the same time, binding of each of the binding partners of eIF4E modulates the kinetics with which it interacts with the other partner. We present structural, kinetic and mutagenesis data that allow us to deduce some of the detailed folding transitions that take place during the eIF4E interactions.

Keywords: translation initiation; eukaryotic initiation factor; protein folding; surface plasmon resonance; NMR

Introduction

Translation initiation on the majority of eukaryotic mRNAs relies on the presence of a cap structure at the 5′ end of the message. This structure is bound by the cap-binding protein eIF4E, which binds also to the adaptor protein eIF4G, which, in turn, can make contact with the ribosomal pre-initiation complex, thus mediating recruitment of the 40 S subunit to the mRNA.[1–3] Formation of the molecular chain 5′cap–eIF4E–eIF4G-MFC-40 S (where MFC is the multi-factor complex comprising eIF1, eIF2, eIF3 and eIF5[4]) is essential for ribosome recruitment to occur, and alterations in the rates of formation and decay of this complex can potentially be used to exert translational control.[5]

The structural analysis of binary cap analog–eIF4E complexes[6,7] revealed that eIF4E in its cap-bound form is a roughly spherical protein with a cleft constituting the cap-binding site, and with an extended N-terminal tail of 35 residues that leaves the body of the protein at a site distal from the cap-binding pocket. This N-terminal tail shows no obvious secondary structure in solution,[7] and cannot be detected in electron density maps of crystals of the full-length protein.[8]

Cap-binding to eIF4E involves two tryptophan residues located inside the cap-binding cleft that hold the double ring of the cap in place *via* π–π stacking interactions.[6,7] The stability of the cap–eIF4E interaction is further enhanced by hydrogen bonds and van der Waals contacts with

Present address: J. D. Gross, Department of Pharmaceutical Chemistry, UCSF, 600 16th Street, S-512E, Box 2280, San Francisco, CA 94143-2280, USA.

Abbreviations used: eIF, eukaryotic initiation factor; HSQC, heteronuclear single quantum coherence; EMSA, electrophoretic mobility-shift assay; MFC, multi-factor complex; SPR, surface plasmon resonance; GST, glutathione-*S*-transferase.

E-mail address of the corresponding author: t.von-der-haar@kent.ac.uk

amino acid residues contained within the cleft. In contrast, binding of eIF4G occurs at a site distal from the cap-binding site, and appears to involve two sets of structural features of eIF4E. A highly conserved primary sequence motif in eIF4G, Tyr-X-X-X-X-Leu-ϕ, where ϕ is Leu, Met or Phe,[9,10] contacts the likewise highly conserved, cap-distal part of the folded body of eIF4E.[10,11] In addition, portions of eIF4G surrounding the minimal binding motif form a doughnut-shaped structure enclosing the extended N-terminal tail of eIF4E and induce the formation of secondary structure elements in the latter.[12]

A number of published observations have suggested that structural changes occur within eIF4E upon cap-binding. Thus, the binding of cap analogs to human, wheat and yeast eIF4E produces changes in CD spectra,[13–16] increases the solubility of the protein *in vitro*,[17] releases the human protein from nuclear bodies *in vivo*,[15] and protects it from proteolytic degradation.[8] The nature of the structural changes during cap-binding has not been well understood, although evaluations of CD difference spectra recorded with human cap-bound and apo-eIF4E suggested that a region involving approximately 40 amino acid residues undergoes large-scale structural rearrangements.[15] Consistent with these findings, analyses of the salt-dependence of the eIF4E:cap interaction revealed that cap-binding also substantially alters the hydration state of the protein.[17]

Taken together, these data indicate that the formation of the cap-binding complex involves a complex interplay of changing conformations in its subunits. In the present study, we explore the nature of these conformational changes and the effect they have on the individual macromolecular interactions within this complex.

Results

Cap-binding induced alterations in NMR spectra of ^{15}N-labeled eIF4E

Both X-ray crystallography and NMR-based structural studies have shown that the largest part of cap-bound eIF4E (ca 178 residues at the C-terminal end) folds into secondary and tertiary structure elements, whereas an N-terminal tail of 35 residues is unstructured.[6–8,17] Upon binding of an eIF4G fragment comprising the eIF4E binding site, the folded part extends about ten more residues towards the N terminus, because an additional segment of ten residues of eIF4E folds into secondary structure elements.[12] However, the overall fold of this protein remains largely unaffected. In order to examine whether the apo-structure of eIF4E differs significantly from the cap-bound structures, we generated cap-free as well as cap-bound, ^{15}N-labeled eIF4E and recorded ^{15}N/^{1}H heteronuclear single quantum coherence (HSQC) spectra for the respective samples (Figure 1).

The ^{15}N/^{1}H correlated spectra for apo-eIF4E are characterized by poor amide ^{1}H chemical-shift dispersion, with many fewer identifiable peaks than has been published for the cap-bound protein (Figure 1(a)).[7] An examination of the backbone NH cross-peaks at low contour threshold reveals the existence of about 100 identifiable cross-peaks, 113 fewer than for the cap-bound protein. The loss of these peaks suggests intermediate timescale motions in the corresponding regions of eIF4E that are broadening the NMR resonances beyond detection. Overall, these data are consistent with the majority of eIF4E being disordered in the absence of the cap structure.

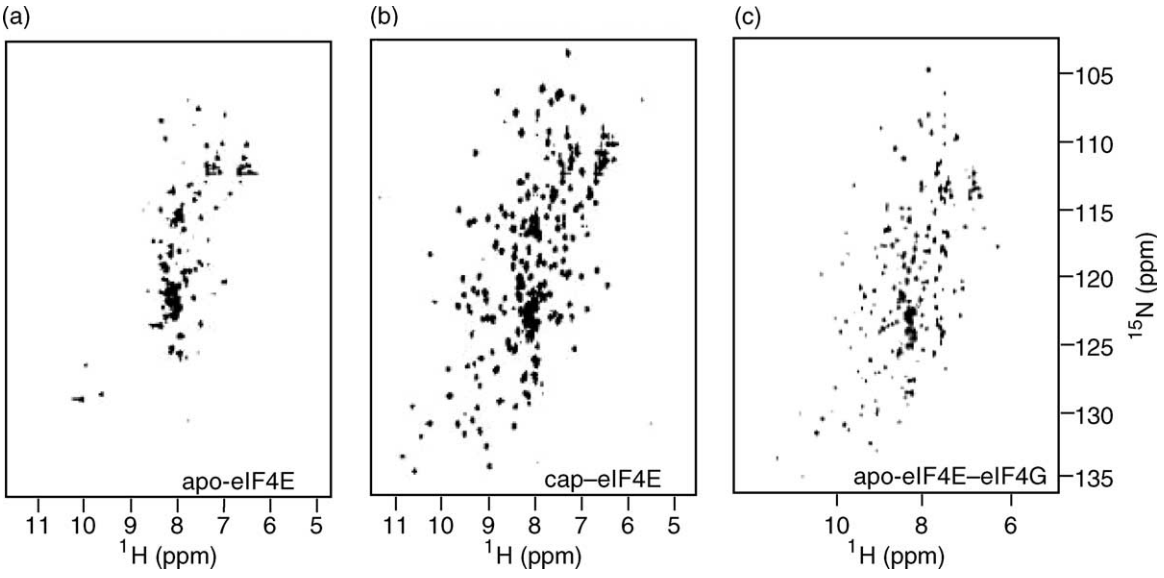

Figure 1. ^{15}N/^{1}H correlated NMR spectra of ^{15}N-labeled *S. cerevisiae* eIF4E (a) in the apo-form, (b) in the presence of m^{7}GDP and (c) in the presence of eIF4G$_{393–490}$.

As the NMR experiments were carried out at pH 6.5, we wanted to investigate whether the disordered state of apo-eIF4E was caused, in part, by this unphysiological pH. CD spectra of cap-free eIF4E were therefore recorded at pH 6.5 and pH 7.5 (data not shown). We observed indistinguishable spectra under the two conditions, indicating that the structural state of apo-eIF4E observed in our NMR experiments is representative of the state that occurs at physiological pH.

In contrast to the spectrum observed with eIF4E alone, addition of a cap analog to our apo-eIF4E preparation generates spectra that are equivalent to those reported for the largely folded cap-bound form of this protein (Figure 1(b)). It appears, therefore, that cap-binding induces the transition of mostly unfolded eIF4E to a folded state.

A qualitative inspection of the spectra in Figure 1 indicates that apo-eIF4E contains a residual folded core. The narrow chemical shift dispersion observed for the cap-free eIF4E spectrum indicates that residual structural elements are likely to be predominantly α-helical, while the extended loss of peak dispersion in the cap-free state indicates loss of the majority of β-sheet structure.

Examining the exact nature of the residual structure of cap-free eIF4E and characterizing its conformation would require assigning the resonances and collecting structural constraints for the approximately 100 resonances that can be observed with apo-eIF4E, which is beyond the scope of the present study. We conclude from this experiment that extensive unfolded-to-folded transitions occur in eIF4E during cap-binding, in regions that remain to be defined exactly.

Cap-binding and eIF4G-binding induce similar unfolded-to-folded transitions in eIF4E

Previous structural work on an m^7GDP–eIF4E–$eIF4G_{393–490}$ complex indicated that eIF4G contacts a highly discontinuous epitope on the dorsal surface of eIF4E.[12] Nevertheless, eIF4G can bind to eIF4E even in the absence of a cap structure. This implies that either the eIF4G binding region is sufficiently folded in apo-eIF4E to be bound by this protein, or that the binding region is unfolded in apo-eIF4E but is induced to assume the correct fold upon contact with eIF4G. In order to distinguish between these two scenarios, we performed an experiment similar to that described above, in which the $^{15}N/^{1}H$ HSQC spectra of free and eIF4G-bound, ^{15}N-labeled apo-eIF4E were compared (Figure 1(c)). Surprisingly, we found that addition of eIF4G to apo-eIF4E results in a spectrum that closely resembles that of cap-bound but eIF4G-free eIF4E (Figure 2). A close inspection of the spectra generated by eIF4E in the cap-bound and eIF4G-bound binary complexes reveals a subset of amino acid residues that show significant chemical shifts between the two states (these are labeled in Figure 2(a)). This subset is composed primarily of amino acid residues in close contact with the cap structure (Figure 2(b)), suggesting that

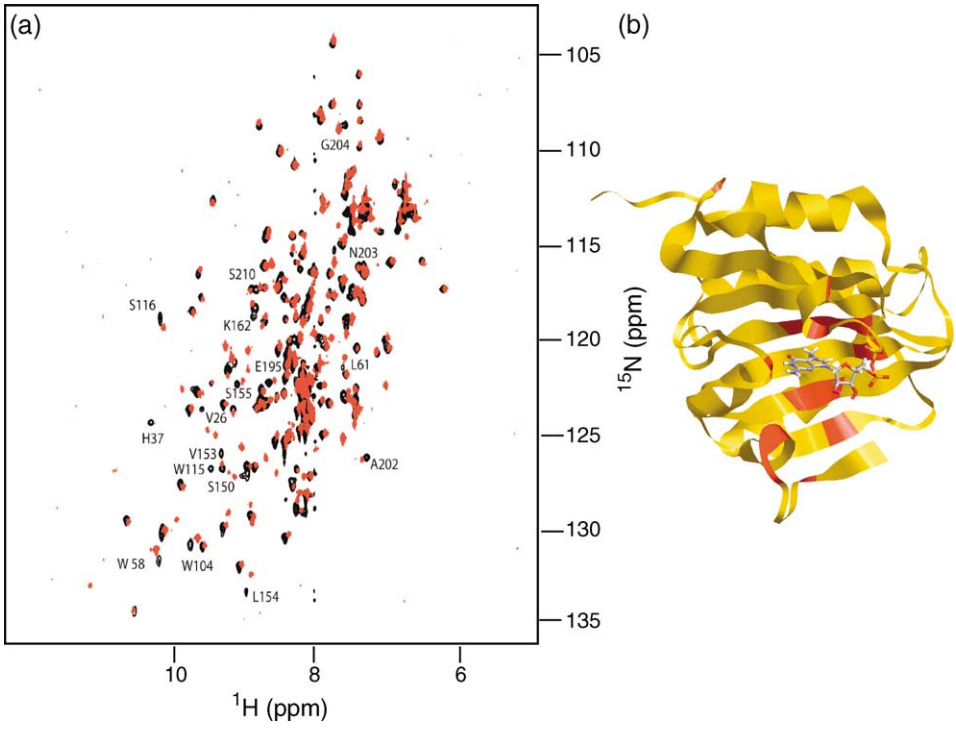

Figure 2. Differences between cap-bound and eIF4G-bound eIF4E. (a) Overlay of eIF4E cross-peaks in the eIF4E-cap (red) and eIF4E–$eIF4G_{393–490}$ (black) binary complexes. The cross-spectra correspond to Figure 1(b) and (c). Cross-peaks showing significant chemical shifts are labeled. (b) Location of the corresponding amino acid residues in the three-dimensional structure of cap-bound eIF4E.

binding of eIF4G to apo-eIF4E induces the latter to assume an overall fold similar to that of the cap-bound state, but with local differences around the cap-binding site. The area around the cap-binding site then adopts its final conformation upon contact with the mRNA cap structure and formation of the ternary cap-eIF4E-eIF4G complex.

The fact that structural features of eIF4E are similar, but not absolutely identical, in the cap-bound and the eIF4G-bound states led us to ask whether conformational changes in this protein during cap-binding might be communicated to eIF4G. We therefore compared spectra obtained with ^{15}N-labeled eIF4G$_{393–490}$ in a binary complex with unlabeled eIF4E, with those for the same protein in a ternary complex with m^{7}GDP and eIF4E. An overlay of the two spectra reveals small shifts in cross-peak positions of the magnitude of 0.1–0.2 ppm (Figure 3(a)), that affect mainly amino acid residues 445–454 and 480–490 (numbering corresponding to full-length yeast eIF4G1). Figure 3(b) shows the location of amino acid residues corresponding to shifted peaks in the context of the m^{7}GDP–eIF4E–eIF4G$_{393–490}$ ternary complex. We interpret the observed shift changes as small changes in the orientation or flexibility of these portions of the eIF4G fragment between the binary and ternary state. In conjunction with the chemical shift changes seen in eIF4E between the cap-bound and eIF4G bound states, we conclude that accommodation of the cap structure in the cap-binding cleft of eIF4E induces minor changes throughout the entire eIF4E:eIF4G$_{393–490}$ complex.

In summary of the data presented so far, our NMR experiments have shown that apo-eIF4E generates NMR spectra typical of a largely unfolded protein, and is induced to adopt a mostly folded conformation upon binding of the cap analog m^{7}GDP. A very similar, extensive conformational change is induced by binding of eIF4G. In contrast, binding of the second binding partner to pre-formed binary complexes (i.e. either binding of eIF4G to cap–eIF4E or binding of cap to eIF4E–eIF4G) leads to chemical shift changes in only small peripheral parts of the cap-binding protein.[12] In the case of the interaction of m^{7}GDP with a binary eIF4E:eIF4G$_{393–490}$ complex, chemical shift changes are visible also in the eIF4G fragment. Any cap-binding-induced conformational changes in the complex therefore correspond to minor adjustments in the structure or flexibility of both eIF4E and eIF4G, rather than the large-scale rearrangements observed with eIF4E alone.

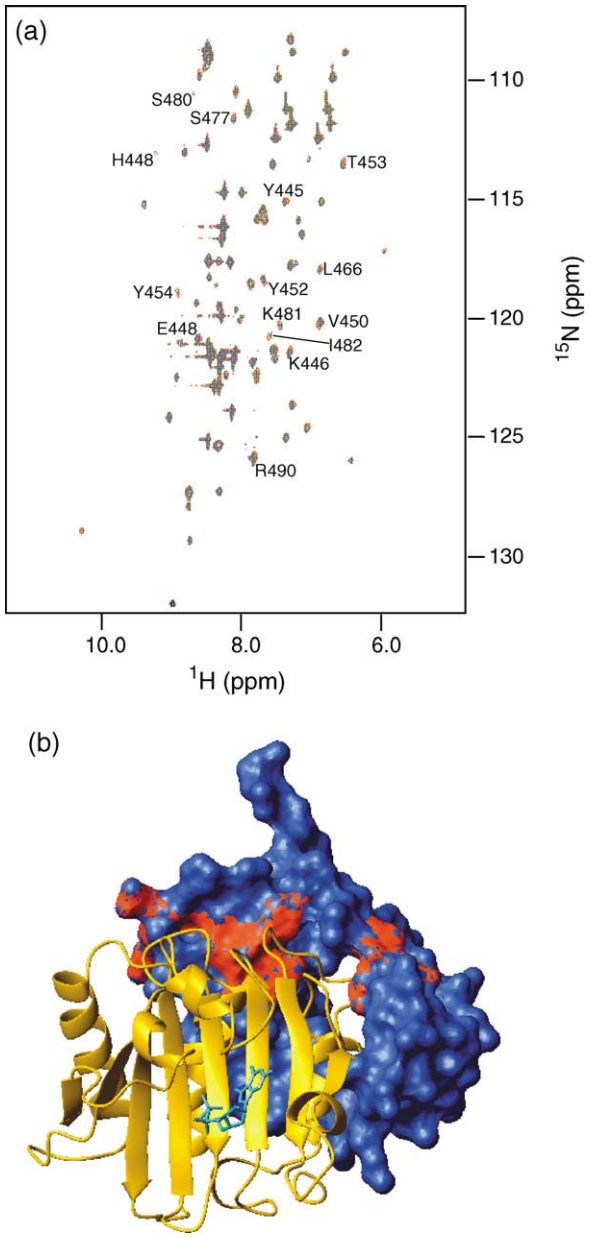

Figure 3. Structural transitions in eIF4G following the binding of the cap analog m^{7}GDP to eIF4G-bound eIF4E. (a) Comparison of the spectra recorded for ^{15}N-labeled eIF4G in complex with apo-eIF4E (red) and cap-bound eIF4E (blue). The numbered amino acid residues are those indicated in red in (b), which shows the three-dimensional structure of an m^{7}GDP–eIF4E–eIF4G$_{393–490}$ ternary complex. The amino acid residues in the eIF4G fragment showing significant shifts upon cap binding are colored red.

Different molecular pathways for the association of eIF4E with eIF4G

Previous work on the association of eIF4G with cap-bound eIF4E indicated that the eIF4G$_{393-490}$ fragment exists in an unstructured state, but folds upon binding to eIF4E.[18] Further work indicated that during the interaction a small part of the unstructured eIF4E N-terminal tail also adopts a helical fold.[12] Binding of eIF4G to cap-bound eIF4E thus involves large folding transitions in eIF4G, and smaller ones in the N-terminal tail of eIF4E. In contrast, our NMR data indicate that binding of eIF4G to apo-eIF4E involves large folding transitions in eIF4E, in addition to those occurring in eIF4G.

In order to investigate whether these differences in association between apo-eIF4E and cap-bound eIF4E with eIF4G become apparent in the kinetics of the respective interactions, we designed an experiment to carefully compare the two using surface plasmon resonance (SPR). Glutathione-*S*-transferase (GST)-eIF4G$_{393–490}$ was covalently immobilized on a BIAcore sensorchip surface, and cap-bound or cap-free eIF4E then injected over this surface. In order to minimize dilution errors, a single dilution series for the different concentrations of eIF4E was prepared, each dilution split in half, and one aliquot supplemented with m^{7}GpppG in eluent buffer while the other was supplemented with an equal volume of eluent buffer only. The regeneration conditions used for dissociation of the formed complexes after each injection (20 mM Hepes (pH 7.5), 6 M guanidinium-HCl) were found not to alter surface performance detectably over a series of ten injection cycles (data not shown).

A comparison of binding curves recorded in the presence and in the absence of cap analog is shown in Figure 4(a). It is immediately apparent that cap-bound eIF4E binds the immobilized eIF4G fragments more rapidly than the apo-form. This difference is particularly evident at intermediate concentrations of eIF4E (compare injections at 10 nM and 20 nM). Moreover, apo-eIF4E-generated sensorgrams (in contrast to those generated with cap-bound eIF4E) do not fit to a two-step binding model of the form:

$$A + B \rightarrow [AB]^* \rightarrow [AB]$$

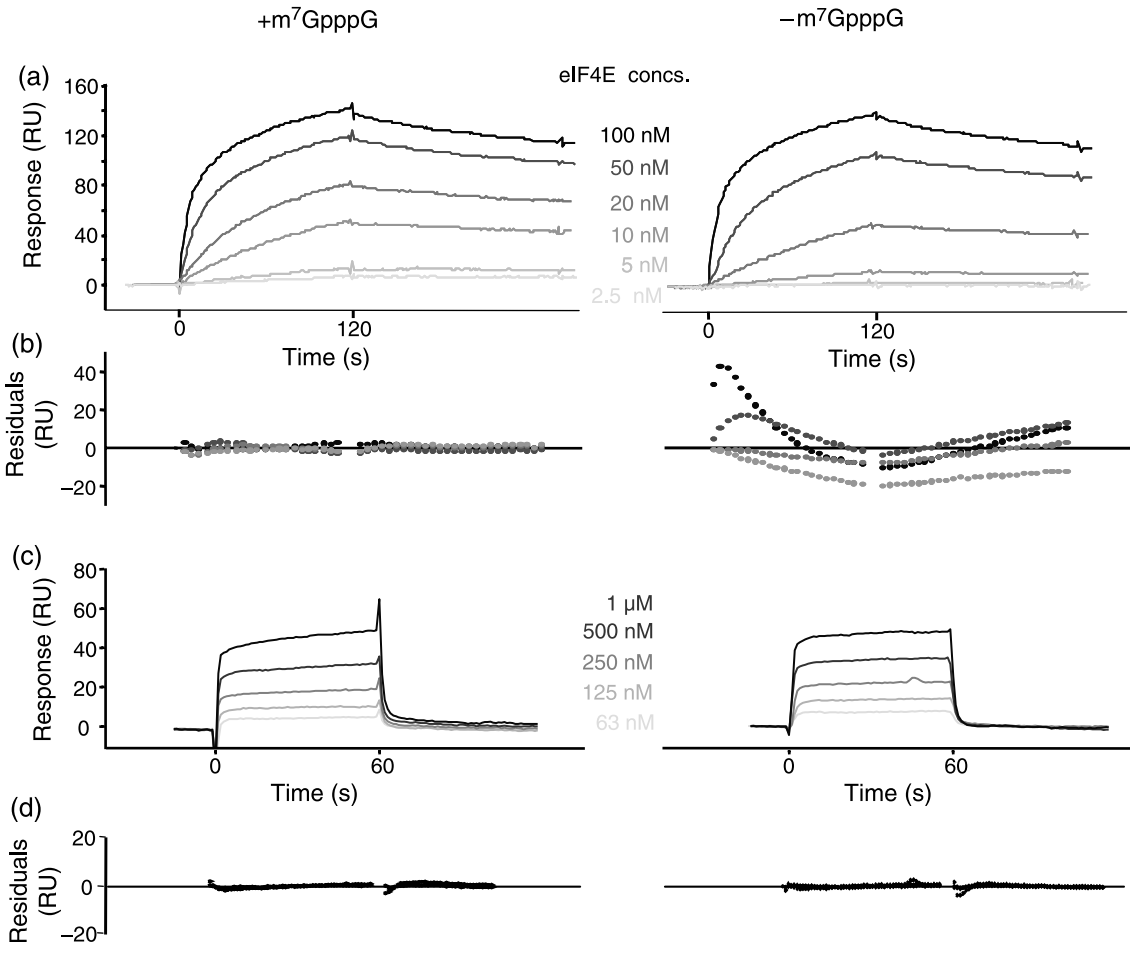

Figure 4. The interaction of eIF4E with GST-eIF4G$_{393–490}$ in the absence or in the presence of the cap analog m^{7}GpppG. Binding curves are recorded from SPR experiments as described in the text. (a) Binding curves for the interactions of full-length eIF4E. The more rapid association in the presence of the cap structure becomes most apparent by comparing the 20 nM and the 10 nM injections. (b) Residuals for fitting the curves in (a) to a two-state binding model of the form:

$$A + B \leftrightarrow AB^* \leftrightarrow AB$$

(see the text for an explanation). (c) Binding curves for the interactions of Δ35 eIF4E. (d) Residuals for fitting the curves in (c) to a simple binding model of the form:

$$A + B \leftrightarrow AB$$

where [AB]* is an intermediate complex that can either decay into its components or undergo a conformational rearrangement to form the final and more stable complex [AB]. While residuals for such a model for cap-bound eIF4E are low ($\chi^2 = 2.0$), residuals for the apo-protein are considerably worse ($\chi^2 = 127$) and show non-random distribution around the *x*-axis (Figure 4(b)). An *F*-test comparing the residuals for separate and combined fits of the two datasets confirms our conclusion derived from visual inspection of the curves, that the binding mechanisms underlying the interactions of apo-eIF4E and cap-bound eIF4E with eIF4G are significantly different ($p \ll 0.001$). Attempts to fit the binding curves to simple Langmuir-binding models of the form $A + B \leftrightarrow [AB]$ result in bad fits for both data sets (χ^2 of 31.3 and 127 for cap-bound eIF4E and apo-eIF4E, respectively), indicating that both forms of eIF4E bind to eIF4G with more complicated binding modes.

An explanation for our inability to obtain good two-state fits for the apo-eIF4E interaction may come from the NMR experiments presented above. In the absence of a cap structure, both eIF4E and $eIF4G_{393–490}$ initiate the interaction in a fully or partly unfolded state, whereas the final complex is largely folded. In this case, there is a greater number of folding intermediates required than in the case of cap-bound eIF4E. If these transitions occur *via* more than one relatively stable intermediate state, the resulting binding curves would not fit to either Langmuir-binding or two-state binding models. In support of this prediction, we find that binding of the Δ35 eIF4E mutant, which can undergo only the first step of the interaction, is much less sensitive to the presence of cap analogs than binding of the wild-type protein. For the interaction of this mutant with $eIF4G_{393–490}$, small differences can be observed in the presence or in the absence of cap analog (Figure 4(c)). Estimates of the kinetic constants for the respective interactions show a slightly slower on-rate in the presence of a cap analog, resulting in a k_D that is reduced by ~10% compared to the cap-free protein. Importantly, however, both interactions show good fits with a simple Langmuir-binding model (Figure 4(d)). This indicates that a very similar initial interaction occurs for both cap-bound and cap-free eIF4E, followed by further steps that appear as a two-step interaction in the case of cap-bound eIF4E, but as a different (possibly more complex) interaction in the case of apo-eIF4E.

Visual inspection of the binding curves observed with wild-type eIF4E also suggests that cap binding alters predominantly later steps of the interaction. This is indicated by the fact that the curves show more dramatic changes at lower concentrations, where formation of the final complexes makes proportionally larger contributions to the sensorgrams; and by direct comparison of the initial slopes of the curves immediately following the start of the injection at the highest concentration of eIF4E.

Molecular mechanism of formation of the eIF4E–eIF4G interface

All the data presented up to this point are consistent with our previously developed idea that the association of eIF4G with cap-bound eIF4E occurs *via* a two-stage reaction,[12] involving at a first stage contacts between eIF4G and the originally identified cap-distal binding site on the folded body of eIF4E.[10,11] In a second stage, parts of eIF4G adopt a mostly α-helical conformation and wrap around the N-terminal tail of eIF4E, thus providing a much enlarged eIF4E–eIF4G binding interface.

We were interested in defining in more detail the involvement of the individual parts of $eIF4G_{393–490}$ in the two interaction stages. Based on the three-dimensional structure of the ternary complex,[12] we selected a number of amino acid residues that were located at the predicted interface between the two proteins and introduced mutations at these points (Figure 5(a)). As controls, we included a previously characterized mutant (Y452A) that does not interact with eIF4E,[19] and a deletion of the N-terminal 35 amino acid residues of eIF4E, which can undergo the initial part of the interaction but cannot undergo the second step, i.e. formation of the extended binding interface.[12]

Figure 5(b) shows SPR sensorgrams for injections of 5 nM and 125 nM eIF4E, respectively, on anti-GST-captured GST-$eIF4G_{393–490}$ for the different combinations of mutant and wild-type proteins. An eIF4E concentration of 5 nM is far below the equilibrium binding constant of 250 nM for the initial interaction, but is above the reported equilibrium constant of 2–4 nM for fully formed complexes.[12] At the lower concentration, a measurable response is produced only if a conversion into the stable, folded complex takes place, whereas for injections at 125 M the initial interaction step makes a significant contribution to the sensorgrams. Comparison of responses at the two concentrations therefore enables us to judge whether an individual mutation affects the initial interaction or the subsequent folding process.

eIF4G W472A is the only mutant that, like Y452A, shows no binding at either concentration, indicating that mutation of W472 impairs the initial contact between the two proteins. All other eIF4G mutants, as well as the eIF4E mutants, show binding profiles with characteristics intermediate between those of the Δ35eIF4E–wteIF4G and wteIF4E–wteIF4G interactions. A more detailed analysis of the sensorgrams indicates that for these mutants the initial interaction can occur with near-wild-type efficiency. Since all of them produce more stable interactions than the Δ35eIF4E–eIF4G complex, we can further conclude that some conversion of the initial complex into a stable complex can take place, but that either the rates of formation or the stability of the final complex are reduced. We also tested a version of eIF4E combining the two individual mutations (K36A and F68A) that were tested for this

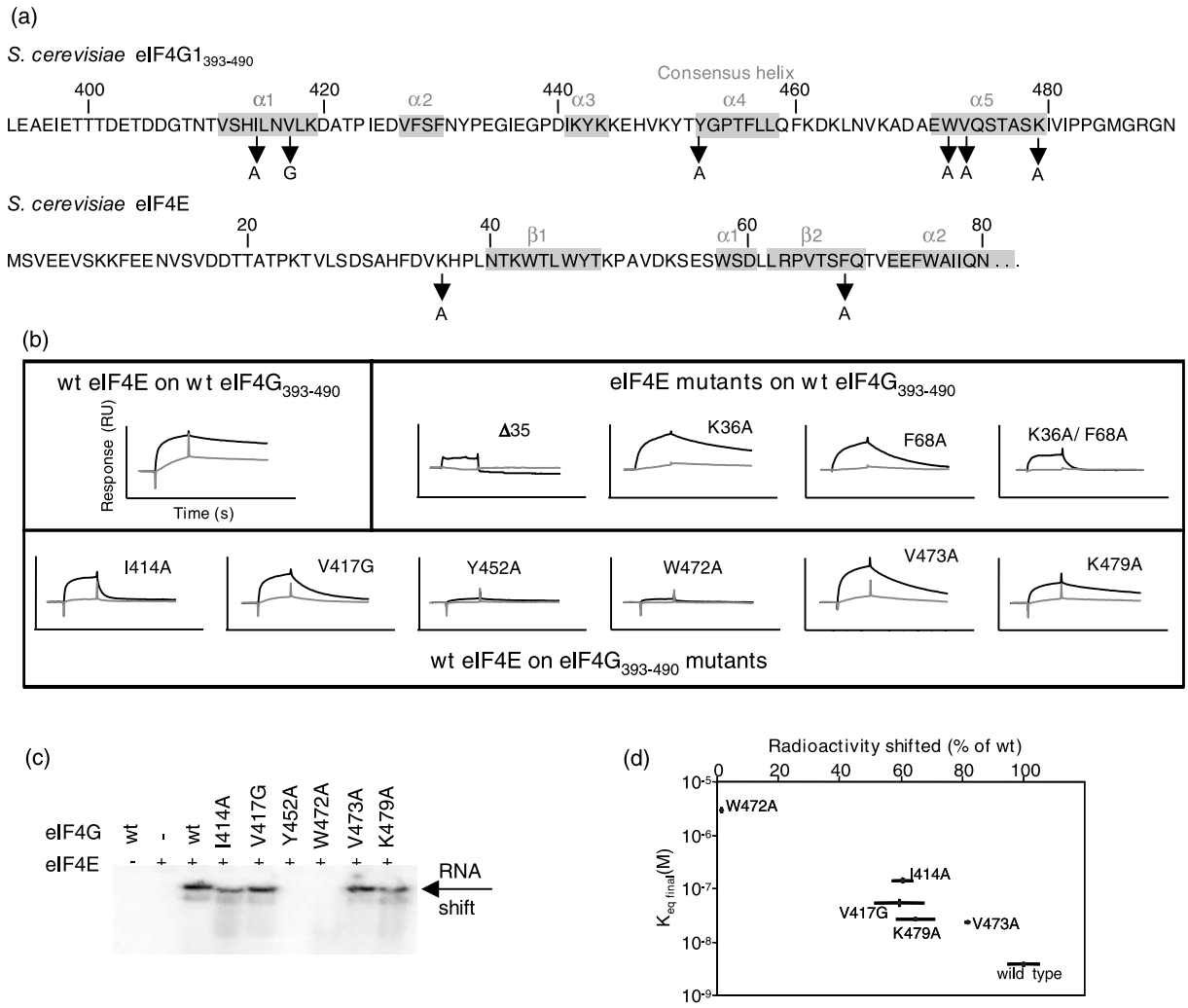

Figure 5. Effects of point mutations on the eIF4E–eIF4G$_{393–490}$ interaction. (a) Positions of the mutations engineered at or near the eIF4E–eIF4G interface. The numbering of secondary structure elements is as described by Gross *et al*.[12] for the eIF4G1 fragment, and as described by Matsuo *et al*.[7] for eIF4E. (b) SPR sensorgrams generated by injecting eIF4E over anti-GST-captured GST-eIF4G$_{393–490}$. eIF4E was injected at 5 nM (grey traces) and 125 nM (black traces). (c) Gel shifts performed with combinations of radiolabeled, capped RNA, eIF4E, and GST-eIF4G$_{393–490}$ mutants. Under the conditions applied for this experiment, eIF4E–RNA complexes appear as bands in the upper part of the gel (indicated by the arrow), whereas free RNA runs off the gel. (d) Quantification of the amount of shifted RNA for each eIF4G mutant, plotted against the estimated equilibrium constant for formation of the final, stable eIF4E–eIF4G complex. Error bars for the amount of shifted RNA represent the standard deviations determined from three independent experiments. Error bars for k_{Eq} values are calculated from the standard deviations of the individual rate constants determined from SPR experiments.

protein, and found that, in this case, the effects of the two mutations were additive, with the combined mutations closely resembling the binding curve for Δ35eIF4E. A summary of rate constants for all interactions extracted from the sensorgrams *via* curve fitting is given in Table 1 (note that for extraction of rate constants from binding curves, injections at four to six different concentrations were used).

In order to confirm the observed effects of the mutations on the second binding step *in vivo*, we generated yeast strains that contained the mutated versions of eIF4E as the only source of this protein. We have previously found that the second binding step is not essential to the functioning of the yeast translational apparatus, since yeast dependent on Δ35eIF4E as their only source of eIF4E are viable.[12] However, the inability of this protein to undergo the second step of the eIF4E–eIF4G interaction produces a weak, slow growth phenotype.[12]

Wild-type eIF4E as well as the K36A, F68A, K36A/F68A and Δ35 mutants of this protein were expressed from a *GAL/PGK1* fusion promoter, which can be regulated by varying the glucose/galactose ratio in the growth medium.[20] This ratio was set to yield eIF4E levels close to those of wild-type yeast.[11] Under these conditions, the eIF4E K36A, F68A single mutations and the K36A/F68A double mutation produced growth rates between those of the wild-type and Δ35eIF4E (Table 1).

Table 1. Rate constants extracted from sensorgrams for eIF4E:eIF4G$_{393–490}$ interactions

	k_{ass1} ($M^{-1}\,s^{-1}$)	k_{diss1} (s^{-1})	k_{ass2} (s^{-1})	k_{diss2} (s^{-1})	k_D (M^{-1})	Growth (%)
Both wt	1.0×10^6	0.12	0.09	0.002	2.3×10^{-9}	100
4E K36A	0.9×10^6	0.10	0.03 ↓	0.006 ↑	7.6×10^{-9}	95
4E F68A	1.2×10^6	0.13	0.05 ↓	0.02 ↑	3.6×10^{-8}	89
4E K36A/F68A	0.8×10^6	0.15	0.02 ↓	0.095 ↑	9.5×10^{-7}	85
4E Δ35	1.3×10^6	0.35 ↑	–	–	2.7×10^{-7}	82
4G I414A	0.7×10^6	0.14	0.004 ↓	0.006 ↑	1.5×10^{-7}	
4G V417G	1.5×10^6	0.15	0.03 ↓	0.018 ↑	5.4×10^{-8}	
4G Y452A	$<10^5$ ↓	>1 ↑	–	–	$>10^{-5}$	
4G W472A	$<10^5$ ↓	>1 ↑	–	–	$>10^{-5}$	
4G V473A	1.4×10^6	0.15	0.07	0.014 ↑	2.4×10^{-8}	
4G K479A	1.5×10^6	0.15	0.02 ↓	0.004 ↑	2.7×10^{-8}	

Arrows indicate changes in rate constants that are significantly different from the wild-type interaction (↑, higher; ↓, lower).

Ranking of the mutants according to the reduction in growth rate yields the same order as ranking according to the calculated reduction in the second interaction step, thus strongly supporting the data generated with the BIAcore system.

Formation of the extensive binding interface during the second step of the interaction has been shown to be a requirement for the arrest of eIF4E on capped mRNAs following eIF4G binding, and for producing detectable signals in RNA gel mobility-shift experiments.[12] We therefore tested our eIF4G mutants for their ability to generate band-shifts of capped, radiolabeled RNAs (Figure 5(c)).

A quantitative analysis of these results shows that there is a strong relationship between the free energy of formation of the binding interface as calculated from:

$$K_{eq\ final} = k_{diss1}/k_{ass1}(k_{diss2}/k_{ass2})$$

and the ability of the complexes to produce signals in the gel mobility-shift assay (Figure 5(d)). A reduction in the amount of shifted RNA is to be expected if either the rates of formation or the thermodynamic stability of the extensive binding interface are reduced. This would lead to lower equilibrium ratios of fully formed *versus* initial complexes with apo-eIF4E, with only the fully formed complexes being able to produce detectable band shifts.

Discussion

Our combined NMR and SPR results suggest that assembly of the cap-binding complex involves large-scale structural rearrangements in both of its protein subunits (Figure 6). Apo-eIF4E is at least partially unfolded, but cap binding causes

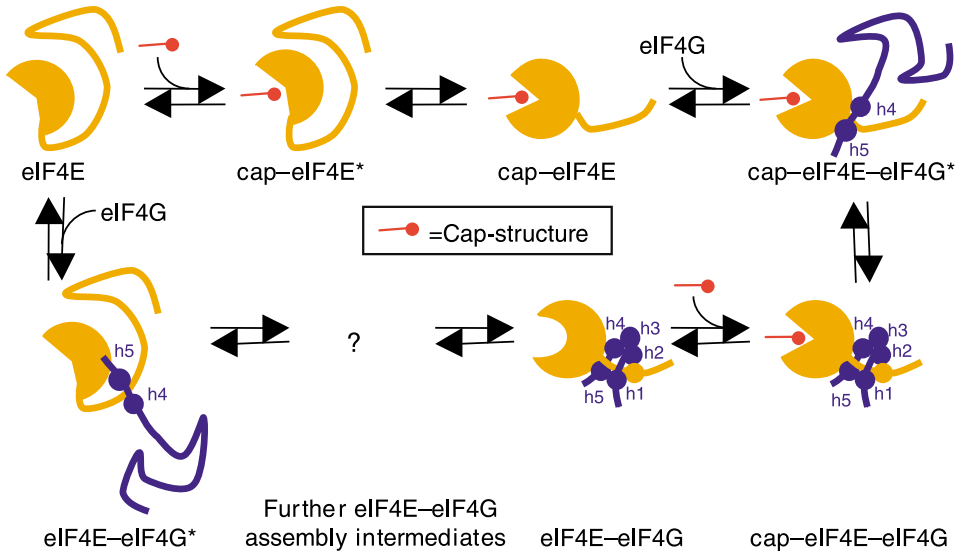

Figure 6. A model of structural transitions during assembly of the cap-bound complex. During the initial cap-binding step (top line), a region of eIF4E undergoes an unfolded-to-folded transition to give the familiar, "cupped-hand" fold of eIF4E. Association of this binary complex with eIF4G$_{393–490}$ is initiated by contacts between helices 4 and 5 with the dorsal surface of eIF4E, followed by formation of the interlocking eIF4E–eIF4G interface through folding of eIF4G$_{393–490}$ helices 1 to 3, and a short helix in the eIF4E N-terminal tail. Binding of eIF4G to apo-eIF4E results in the formation of similar secondary structure elements in both proteins as in the cap-bound state, although small differences exist between the cap-bound and unbound complexes. The folding pathway that leads to formation of apo-eIF4E–eIF4G is unclear.

the protein to adopt its previously published, largely folded conformation. Moreover, eIF4G-binding induces folding of apo-eIF4E to a structure similar to, but not identical with, that assumed upon cap-binding.

A large-scale folding event occurs also in the eIF4G fragment upon binding to eIF4E.[12,18] The analysis of mutations in both eIF4E and eIF4G described here allows us to deduce information about the order of events during this structural transition (see Figure 6). All mutations affecting the initial interaction are either located in the dorsal part of the folded body of eIF4E or make contacts with this region, namely the eIF4E P38, V71 and W75 mutants described in an earlier study,[11] and the eIF4G Y452 and W472 mutants described here (Figure 5). It is interesting to note that helix 4 of $eIF4G_{393–490}$, the so-called consensus helix containing the minimal eIF4E-binding motif including Y453, is alone able to bind to eIF4E.[10] The W472 residue is situated 14 amino acid residues towards the C terminus of this helix, but its mutation can nevertheless prevent any interaction with eIF4E. As the exchange from tryptophan to alanine does not alter the charge of the mutated region significantly, we can exclude electrostatic effects as the reason for the impaired interaction. The inability to bind may therefore rather be caused by effects of the W to A exchange on the propensity to form secondary structure elements in the surrounding region. Independently of the molecular mechanism that prevents the W472 mutant from binding to eIF4E, we can conclude that the consensus helix behaves differently in the context of the full-length protein compared to the isolated peptide. Identified eIF4G contact points with eIF4E that are important for the initial interaction therefore involve helix 4 and the N terminus of helix 5 (numbering as described by Gross *et al*.[12]).

Most of the mutants affecting formation or stability of the extended binding interface are located in, or make contact with, the N-terminal tail of eIF4E. This is consistent with the observation that the N-terminal tail is required to induce the folding of the eIF4G fragment into secondary and tertiary structure elements.[12] Interesting exceptions to this rule are eIF4E F68 and eIF4G V473 (Figure 5). The V473 mutation is located in the middle of helix 5, and makes contact with the F68 residue in eIF4E. Although this contacting pair is located adjacent to the W472 residue involved in the initial step of the interaction, it clearly is of much less importance for the initial interaction than the tryptophan. There is also no contact between this pair and other residues that seems likely to be important for the second interaction step. However, the V473–F68 pairing, while dispensable for the initial interaction to occur, may be required for correct formation or orientation of eIF4G helix 5, which in turn is required for induction of the subsequent formation of helix 1. In conclusion, the second step of the cap–eIF4E–eIF4G interaction involves the formation of $eIF4G_{393–490}$ helices 1–3, the wrapping of this part of eIF4G around the eIF4E N-terminal tail, and formation of the short helix within this part of eIF4E.

The fact that the interactions of free and cap-bound eIF4E with eIF4G differ kinetically (Figure 4) suggests that distinct intermediate states may exist for apo-eIF4E compared to the 5′ cap–eIF4E complex. This is not surprising given that the interaction between the apo-proteins involves large-scale structural rearrangements in both eIF4E and eIF4G, while the interaction in the presence of a cap analog involves such changes only in the latter. Despite clear differences in the folding pathways, our NMR experiments suggest that the complexes attained at the end of these pathways differ only minimally. Characterization of the details of the different folding trajectories and intermediate eIF4E–eIF4G complex(es) that form in the presence and in the absence of the cap structure represents an interesting challenge for the future.

Finally, the biological significance of the described structural changes in eIF4E and eIF4G upon cap-binding may be to enable ribosomal complexes to distinguish between the respective cap-associated and cap-free eIF4G–eIF4E complexes. Preferential binding to mRNA-associated eIF4G would be particularly important if the level of 43 S available for recruitment to mRNAs is relatively low, since in this case any "unproductive" contacts with free eIF4G would reduce the rate of "productive" contacts with mRNAs. Alternatively, contacts with cap-bound eIF4E–eIF4G complexes may signal proximity to the mRNA 5′-end and thus be important for start-codon selection. Possibly relevant here is a recent report that mammalian eIF4F can prevent eIF5-promoted GTP hydrolysis in 43 S complexes in the presence of cap analogs, but not in the cap-free form.[21] In a wider context, the folding transitions described here reaffirm the biological significance of extensive unstructured regions in a diverse range of natural proteins.[22]

Materials and Methods

Plasmids, strains and protein expression

eIF4E,[14] GST-$eIF4G_{393–490}$ fragment[12] and mutant versions of eIF4E or the $eIF4G_{393-490}$ fragment,[23] were generated as described. Wild-type and mutant eIF4E was synthesized under control of the *GPF* promoter[20] in the *S. cerevisiae* strain Mat**a** *cdc33*::*LEU2 leu2 ura3 trp*.[24]

Surface plasmon resonance experiments

For all BIAcore experiments, GST-tagged eIF4G fragment was immobilized on the surfaces of CM5 sensorchips (BIAcore), and eIF4E injected to observe the interactions.

For the sensorgrams in Figure 4, GST-$eIF4G_{393–490}$ was covalently coupled to the dextran matrix using the BIAcore amine coupling kit. A control surface was created by coupling unfused GST. Coupling conditions for both proteins were 30 μg/ml at a coupling pH of 4.5.

For all other experiments, anti-GST antibodies from the BIAcore GST capture kit were covalently coupled to a sensorchip surface according to the manufacturer's instructions. GST-fused eIF4G fragment was then captured on these antibodies by injections at 1 μg/ml in eluent buffer. Control surfaces were created by capturing unfused GST.

eIF4E was dialyzed overnight against 500–1000 volumes of eluent buffer (50 mM Hepes (pH 7.5), 100 mM NaCl, 5 mM $MgCl_2$, 0.005% (v/v) surfactant p20). Following dialysis, the dialysis buffer itself was sterile-filtered and used as eluent buffer in order to minimize bulk refractive index changes. Association of eIF4E with the eIF4G fragments was observed using the "Kinject" procedure with association and dissociation times of 2 min each, and flow rates of 75 μl/min. Regeneration conditions were 30 s injections of 20 mM Hepes (pH 7.5) 6 M guanidine-HCl, to strip eIF4E from the covalently bound eIF4G fragments. In the case of the anti-GST captured eIF4G, surfaces were regenerated by two consecutive injections of 10 mM glycine at pH 2.

For data analysis, the interaction of eIF4E with GST was subtracted from interactions with the GST-eIF4G fusions. Resulting curves were then analyzed by performing global or local fittings with the BIAevaluation software (v 4.1), using the pre-programmed Langmuir and two-state models of the software. For all fittings, the RI value was set as a constant with value zero. Where possible, R_{Max} values were verified independently of the fitting procedure by saturating the chip surfaces through injections of high concentrations of eIF4E.

NMR

eIF4E, $eIF4G_{393–490}$ and eIF4E–$eIF4G_{393–490}$ were expressed using M9 medium with $^{15}NH_4Cl$ as the sole nitrogen source. Generation of apo-eIF4E and apo-eIF4E–$eIF4G_{393–490}$ was performed as described.[12] Apo-eIF4E–$eIF4G_{393–490}$ was further purified on a HiLoad G75 gel-filtration column (Amersham-Pharmacia) to ensure 1:1 stoichiometry. HSQC experiments were performed on a Varian Inova 600 MHz spectrometer with (apo-eIF4E) or without (apo-eIF4E–$4G_{393–490}$) a cold-probe accessory in buffer conditions as described[7] but without the Chaps. Concentrations of apo-eIF4E, m^7GDP–eIF4E and apo-eIF4E–$eIF4G_{393–490}$ complex were approximately 0.1 mM, 0.5 mM and 0.250 mM, respectively.

Acknowledgements

J.E.G.M. thanks the Wellcome Trust (UK) and the Biotechnology and Biological Sciences Research Council (BBSRC, UK) for funding, and acknowledges the support of a Wolfson-Royal Society Research Fellowship. J.D.G. is grateful for start-up funds from the University of Massachusetts Medical School and a Research-Scholar Award from the Worcester Foundation for Biomedical Research. G.W. thanks the National Institutes of Health for support (grant CA68262). T.v.d.H. is recipient of a Wellcome Trust (UK) Research Career Development Fellowship (grant 075438/Z/04/Z).

References

1. Hershey, J. W. B. & Merrick, W. C. (2000). Pathway and mechanism of initiation of protein synthesis. In *Translational Control of Gene Expression* (Sonenberg, N., Hershey, J. W. B. & Mathews, M. B., eds), pp. 33–88, Cold Spring Harbor Laboratory Press, Cold Spring Harbor, NY.
2. McCarthy, J. E. G. (1998). Posttranscriptional control of gene expression in yeast. *Microbiol. Mol. Biol. Rev.* **62**, 1492–1553.
3. Kapp, L. D. & Lorsch, J. R. (2004). The molecular mechanics of eukaryotic translation. *Annu. Rev. Biochem.* **73**, 657–704.
4. Asano, K., Clayton, J., Shalev, A. & Hinnebusch, A. G. (2000). A multifactor complex of eukaryotic initiation factors, eIF1, eIF2, eIF3, eIF5, and initiator tRNA(Met) is an important translation initiation intermediate *in vivo*. *Genes Dev.* **14**, 2534–2546.
5. von der Haar, T., Gross, J. D., Wagner, G. & McCarthy, J. E. G. (2004). The mRNA cap-binding protein eIF4E in post-transcriptional gene expression. *Nature Struct. Mol. Biol.* **11**, 503–511.
6. Marcotrigiano, J., Gingras, A. C., Sonenberg, N. & Burley, S. K. (1997). Cocrystal structure of the messenger RNA 5′ cap-binding protein (eIF4E) bound to 7-methyl-GDP. *Cell*, **89**, 951–961.
7. Matsuo, H., Li, H., McGuire, A. M., Fletcher, C. M., Gingras, A. C., Sonenberg, N. & Wagner, G. (1997). Structure of translation factor eIF4E bound to m^7GDP and interaction with 4E-binding protein. *Nature Struct. Biol.* **4**, 717–724.
8. Tomoo, K., Shen, X., Okabe, K., Nozoe, Y., Fukuhara, S., Morino, S. *et al*. (2003). Structural features of human initiation factor 4E, studied by X-ray crystal analyses and molecular dynamics simulations. *J. Mol. Biol.* **328**, 365–383.
9. Altmann, M., Schmitz, N., Berset, C. & Trachsel, H. (1997). A novel inhibitor of cap-dependent translation initiation in yeast: p20 competes with eIF4G for binding to eIF4E. *EMBO J.* **16**, 1114–1121.
10. Marcotrigiano, J., Gingras, A. C., Sonenberg, N. & Burley, S. K. (1999). Cap-dependent translation initiation in eukaryotes is regulated by a molecular mimic of eIF4G. *Mol. Cell*, **3**, 707–716.
11. Ptushkina, M., von der Haar, T., Vasilescu, S., Frank, R., Birkenhäger, R. & McCarthy, J. E. G. (1998). Cooperative modulation by eIF4G of eIF4E-binding to the mRNA 5′ cap in yeast involves a site partially shared by p20. *EMBO J.* **17**, 4798–4808.
12. Gross, J. D., Moerke, N. J., von der Haar, T., Lugovskoy, A. A., Sachs, A. B., McCarthy, J. E. G. & Wagner, G. (2003). Ribosome loading onto the mRNA cap is driven by conformational coupling between eIF4G and eIF4E. *Cell*, **115**, 739–750.
13. Wang, Y., Sha, M., Ren, W. Y., van Heerden, A., Browning, K. S. & Goss, D. J. (1996). pH-dependent and ligand induced conformational changes of eucaryotic protein synthesis initiation factor eIF-(iso)4F: a circular dichroism study. *Biochim. Biophys. Acta*, **1297**, 207–213.
14. von der Haar, T., Ball, P. D. & McCarthy, J. E. G. (2000). Stabilization of eukaryotic initiation factor 4E binding to the mRNA 5′-Cap by domains of eIF4G. *J. Biol. Chem.* **275**, 30551–30555.
15. Cohen, N., Sharma, M., Kentsis, A., Perez, J. M., Strudwick, S. & Borden, K. L. (2001). PML RING suppresses oncogenic transformation by reducing the affinity of eIF4E for mRNA. *EMBO J.* **20**, 4547–4559.

16. McCubbin, W. D., Edery, I., Altmann, M., Sonenberg, N. & Kay, C. M. (1988). Circular dichroism and fluorescence studies on protein synthesis initiation factor eIF-4E and two mutant forms from the yeast *Saccharomyces cerevisiae*. *J. Biol. Chem.* **263**, 17663–17671.
17. Niedzwiecka, A., Marcotrigiano, J., Stepinski, J., Jankowska-Anyszka, M., Wyslouch-Cieszynska, A., Dadlez, M. *et al*. (2002). Biophysical studies of eIF4E cap-binding protein: recognition of mRNA 5′ cap structure and synthetic fragments of eIF4G and 4E-BP1 proteins. *J. Mol. Biol.* **319**, 615–635.
18. Hershey, P. E. C., McWhirter, S. M., Gross, J. D., Wagner, G., Alber, T. & Sachs, A. B. (1999). The Cap-binding protein eIF4E promotes folding of a functional domain of yeast translation initiation factor eIF4G1. *J. Biol. Chem.* **274**, 21297–21304.
19. Tarun, S. Z., Jr, Wells, S. E., Deardorff, J. A. & Sachs, A. B. (1997). Translation initiation factor eIF4G mediates *in vitro* poly(A) tail-dependent translation. *Proc. Natl Acad. Sci. USA*, **94**, 9046–9051.
20. Oliveira, C. C., van den Heuvel, J. J. & McCarthy, J. E. G. (1993). Inhibition of translational initiation in *Saccharomyces cerevisiae* by secondary structure: the roles of the stability and position of stem-loops in the mRNA leader. *Mol. Microbiol.* **9**, 521–532.
21. Majumdar, R. & Maitra, U. (2005). Regulation of GTP hydrolysis prior to ribosomal AUG selection during eukaryotic translation initiation. *EMBO J.* **24**, 3737–3746.
22. Dyson, H. J. & Wright, P. E. (2005). Intrinsically unstructured proteins and their functions. *Nat. Rev. Mol. Cell. Biol.* **6**, 197–208.
23. Mikaelian, I. & Sergeant, A. (1992). A general and fast method to generate multiple site directed mutations. *Nucl. Acids Res.* **20**, 376.
24. Altmann, M. & Trachsel, H. (1989). Altered mRNA cap recognition activity of initiation factor 4E in the yeast cell cycle division mutant cdc33. *Nucl. Acids Res.* **17**, 5923–5931.

Edited by D. E. Draper

(Received 19 September 2005; received in revised form 9 December 2005; accepted 10 December 2005)
Available online 27 December 2005